The HST/ACS Coma Cluster Survey: I - Survey Objectives and Design[1]

David Carter[2], Paul Goudfrooij[3], Bahram Mobasher[3], Henry C. Ferguson[3], Thomas H. Puzia[4], Alfonso L. Aguerri[5], Marc Balcells[5], Dan Batcheldor[6], Terry J. Bridges[7], Jonathan I. Davies[8], Peter Erwin[9,10], Alister W. Graham[11], Rafael Guzmán[12], Derek Hammer[13], Ann Hornschemeier[14], Carlos Hoyos[12,29], Michael J. Hudson[15], Avon Huxor[16], Shardha Jogee[17], Yutaka Komiyama[18], Jennifer Lotz[19], John R. Lucey[20], Ronald O. Marzke[21], David Merritt[6], Bryan W. Miller[22], Neal A. Miller[13,23], Mustapha Mouhcine[2], Sadanori Okamura[24], Reynier F. Peletier[25], Steven Phillipps[16], Bianca M. Poggianti[26], Ray M. Sharples[19], Russell J. Smith[19], Neil Trentham[27], R. Brent Tully[28], Edwin Valentijn[25], Gijs Verdoes Kleijn[25]

[1]Based on observations with the NASA/ESA *Hubble Space Telescope* obtained at the Space Telescope Science Institute, which is operated by the association of Universities for Research in Astronomy, Inc., under NASA contract NAS 5-26555. These obervations are associated with program GO10861.

[2]Astrophysics Research Institute, Liverpool John Moores University, Twelve Quays House, Egerton Wharf, Birkenhead CH41 1LD, UK.

[3]Space Telescope Science Institute, 3700 San Martin Drive, Baltimore, MD 21218, USA.

[4]Dominion Astrophysical Observatory, Herzberg Institute of Astrophysics, National Research Council of Canada, 5071 West Saanich Road, Victoria, BC V9E 2E7, Canada.

[5]Instituto de Astrofísica de Canarias, C/Vía Lactea s/n, 38200 La Laguna, Tenerife, Spain.

[6]Department of Physics, Rochester Institute of Technology, 85 Lomb Memorial Drive, Rochester, NY 14623, USA.

[7]Department of Physics, Engineering Physics and Astronomy, Queen's University, Kingston, Ontario K7L 3N6, Canada.

[8]School of Physics and Astronomy, Cardiff University, The Parade, Cardiff CF24 3YB, UK.

[9]Max-Planck-Institut für Extraterrestrische Physik, Giessenbachstrasse, D-85748 Garching, Germany.

[10]Universitäts-Sternwarte München, Scheinerstrasse 1, D-81679 München, Germany

[11]Centre for Astrophysics and Supercomputing, Swinburne University of Technology, Hawthorn, VIC 3122, Australia.

[12]Department of Astronomy, University of Florida, PO Box 112055, Gainesville, FL 32611, USA.

[13]Department of Physics and Astronomy, Johns Hopkins University, 3400 North Charles Street, Baltimore, MD 21218, USA.

[14]Laboratory for X-Ray Astrophysics, NASA Goddard Space Flight Center, Code 662.0, Greenbelt, MD 20771, USA.

[15]Department of Physics and Astronomy, University of Waterloo, 200 University Avenue West, Waterloo, Ontario N2L 3G1, Canada.

[16]Astrophysics Group, H.H. Wills Physics Laboratory, University of Bristol, Tyndall Avenue, Bristol BS8 1TL, UK.

[17]Department of Astronomy, University of Texas at Austin, 1 University Station C1400, Austin, TX 78712, USA.

[18]Subaru Telescope, National Astronomical Observatory of Japan, 650 North A'ohoku Place, Hilo, HI 96720, USA.

[19]Leo Goldberg Fellow, National Optical Astronomy Observatory, 950 North Cherry Avenue, Tucson, AZ 85719, USA.

[20]Department of Physics, University of Durham, South Road, Durham DH1 3LE, UK.

[21]Department of Physics and Astronomy, San Francisco State University, San Francisco, CA 94132-4163,

ABSTRACT

We describe the HST ACS Coma cluster Treasury survey, a deep two-passband imaging survey of one of the nearest rich clusters of galaxies, the Coma cluster (Abell 1656).

The survey was designed to cover an area of 740 arcmin^2 in regions of different density of both galaxies and intergalactic medium within the cluster. The ACS failure of January 27th 2007 leaves the survey 28% complete, with 21 ACS pointings (230 arcmin^2) complete, and partial data for a further 4 pointings (44 arcmin^2).

Predicted survey depth for 10σ detections for optimal photometry of point sources is $g' = 27.6$ in the F475W filter, and I_C=26.8 mag in F814 (AB magnitudes). Initial simulations with artificially injected point sources show 90% recovered at magnitude limits of $g' = 27.55$ and $I_C = 26.65$. For extended sources, the predicted 10σ limits for a 1 arcsecond^2 region are $g' = 25.8$ mag arcsec^{-2} and $I_C = 25.0$ mag arcsec^{-2}.

We highlight several motivating science goals of the survey, including study of the faint end of the cluster galaxy luminosity function, structural parameters of dwarf galaxies, stellar populations and their effect on colors and color gradients, evolution of morphological components in a dense environment, the nature of ultra compact dwarf galaxies, and globular cluster populations of cluster galaxies of a range of luminosities and types. This survey will also provide a local rich

---

USA.

[22]Gemini Observatory, Casilla 603, La Serena, Chile.

[23]Jansky Fellow of the National Radio Astronomy Observatory. The National Radio Astronomy Observatory is a facility of the National Science Foundation operated under cooperative agreement by Associated Universities, Inc.

[24]Department of Astronomy, University of Tokyo, 7-3-1 Hongo, Bunkyo, Tokyo 113-0033, Japan.

[25]Kapteyn Astronomical Institute, University of Groningen, PO Box 800, 9700 AV Groningen, The Netherlands.

[26]INAF-Osservatorio Astronomico di Padova, Vicolo dell'Osservatorio 5, Padova I-35122, Italy.

[27]Institute of Astronomy, Madingley Road, Cambridge CB3 0HA, UK.

[28]Institute for Astronomy, University of Hawaii, 2680 Woodlawn Drive, Honolulu, HI 96822, USA.

[29]Departamento de Física Teórica, Universidad Autónoma de Madrid, Carretera de Colmenar Viejo km 15.600, 28049 Madrid, Spain

cluster benchmark for various well known *global* scaling relations and explore new relations pertaining to the *nuclear* properties of galaxies.

Subject headings: galaxies: clusters: individual (Abell 1656) — galaxies: fundamental parameters — galaxies: photometry — galaxies: stellar content — galaxies: structure — galaxies: luminosity function

1. Introduction and background

The Coma cluster of galaxies, Abell 1656, is along with the Perseus cluster the nearest rich, and dense cluster environment. Unlike the Perseus cluster, it is at high galactic latitude (b = 87.9°) and it has been a popular target for study at all wavelengths. Progressively deeper wide-area photometric surveys of Coma have become available over the past 30 years, and waveband coverage has spread from the original B and V band surveys into the near ultra-violet and infra-red (Godwin & Peach 1977; Godwin, Metcalfe & Peach 1983 (GMP); Komiyama et al. 2002; Adami et al. 2006; Eisenhardt et al. 2007). A larger area around Coma is covered by the imaging part of Data Release 5 of the Sloan Digital Sky Survey (Adelman-McCarthy et al. 2007). From these surveys, samples of galaxies have been selected for spectroscopic study, which has resulted in an understanding of the internal dynamics of the cluster (Colless & Dunn 1996; Mobasher et al. 2001; Edwards et al. 2002; Gutierrez et al. 2004), the internal dynamics of cluster members (Lucey et al. 1991; Jorgensen et al. 1996; Smith et al. 2004; Matkovic & Guzmán 2005; Cody et al. 2007), and their mean luminosity weighted stellar ages, abundances and α-enhancement (Bower et al. 1992a,b; Guzmán et al. 1992; Caldwell et al. 1993; Jorgensen 1999; Poggianti et al. 2001; Moore et al. 2002; Nelan et al. 2005; Smith et al. 2006; Matkovic et al. 2007). Coma presents us with the best opportunity to study large samples of galaxies of different luminosity, environment and morphological type, but at a common distance, and with a common Galactic extinction.

There is good agreement on the distance to the Coma cluster, with independent studies using six different methods yielding values in the range 84 – 108 Mpc, as summarised in Table 1. These values fit well with the current concordance cosmology: assuming $H_0 = 71$ km/s/Mpc; $\Omega_\lambda = 0.73$; $\Omega_m = 0.27$, and a redshift z = 0.0231 gives a distance of 99.3 Mpc. In this paper we assume a distance of 100 Mpc, equivalent to a distance modulus of 35.00.

Table 1. The Distance to Coma determined by different techniques

Technique	Distance (Mpc)	Distance Modulus	Reference
I-band Tully-Fisher	86.3±6	34.68±0.15	Tully & Pierce (2000)
K′-band SBF	85±10	34.64±0.27	Jensen et al. (1999)
I-band SBF	102±14	35.04±0.32	Thomsen et al. (1997)
$D_n - \sigma$	96±6	34.90±0.14	Gregg (1997)
Fundamental Plane	108±12	35.16±0.25	Hjorth & Tanvir (1997)
Globular Cluster LF	102±6	35.05±0.12	Kavelaars et al. (2000)

Coma lies in a rich region of the large-scale distribution of galaxies, at the intersection of a number of filaments. Figure 1 shows two projections of the distribution of galaxies in supergalactic co-ordinates in the region of Coma and the nearby richness class 2 cluster Abell 1367. The Great Wall (Geller & Huchra 1989) a vertical structure in the two panels of Figure 1, runs through these two clusters, other filaments intersect the Great Wall at the Coma cluster.

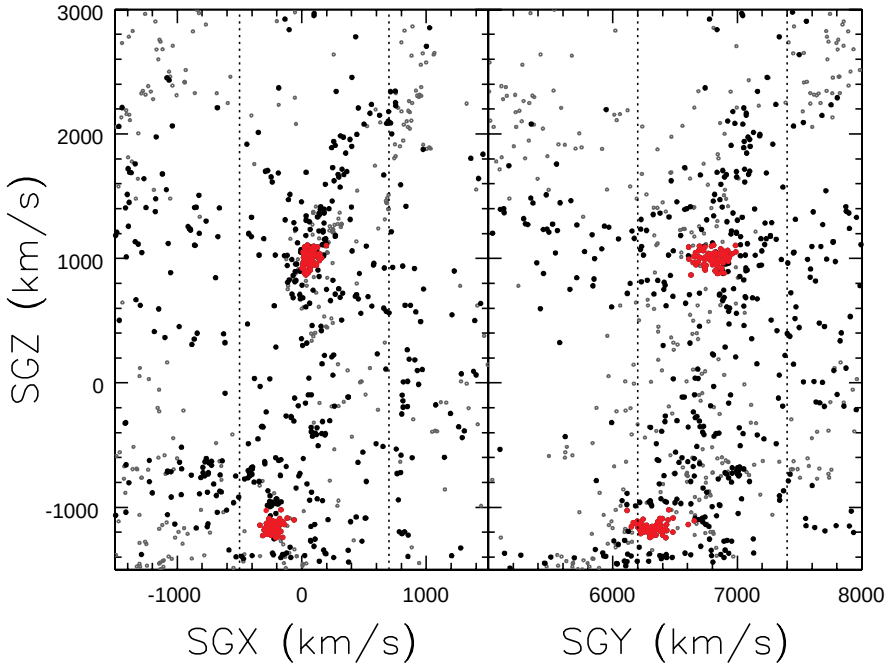

Fig. 1.— The location and environment of the Coma cluster in supergalactic co-ordinates. The left panel shows a projection onto supergalactic Y, close to the plane of the sky. The right panel shows a projection onto supergalactic X, in this panel the horizontal (Y) axis is close to measured redshift. All axes are in equivalent cz. Positions of the points are derived from measured sky positions and redshifts. Members of Coma (centre) and Abell 1367 (bottom) are plotted as filled red circles, for these galaxies the redshift used to compute the distance is the cluster redshift, with a random velocity offset chosen to make the cluster appear round. For non cluster members, measured cz is used, and the positions are plotted as filled black circles if they have velocities within ±600 km/s of the Coma mean in the depth dimension in that particular panel, and as open grey circles otherwise. The Great Wall is the structure at SGY $\sim$ 6800 km/s in the right panel and is seen face on in the left panel

There is a uniquely rich multi-wavelength dataset on the Coma cluster. X-ray observations covering a large area of the cluster have been made with ROSAT (White et al. 1993) and XMM-Newton (Briel et al. 2001), showing the distribution and properties of the hot intra-cluster medium (ICM), and X-ray properties of individual galaxies have been studied by Finoguenov et al. (2004) and by Hornschemeier et al. (2006). Coma has been shown by INTEGRAL to be an extended hard X-ray/soft γ-ray source (Renaud et al. 2006). At soft X-ray and Extreme Ultraviolet wavelengths there is a thermal excess (Lieu et al. 1996; Kaastra et al. 2003; Bonamente et al. 2003; Bowyer et al. 2004). GALEX has been used to observe the cluster in the mid and near Ultraviolet and has sufficient spatial resolution to measure the UV properties of individual galaxies. In the infra-red, studies of the galaxies have been made using SPITZER, both with IRAC at 3.6 - 8 μm (Jenkins et al. 2007) and with MIPS at 24 and 70 μm (Bai et al. 2006). At radio wavelengths, VLA continuum maps cover much of the cluster (Miller et al. in preparation), and in the HI 21 cm line there are extensive VLA imaging surveys (Bravo-Alfaro et al. 2000, 2001), and single-dish spectra and fluxes for samples of spiral galaxies (Gavazzi et al. 2006; Vogt et al. 2004).

This wealth of existing data makes Coma a prime target for studies of the origin and evolution of the galaxy content of clusters, and of its interaction with the other components (gas and dark matter). Moreover, as the richest and best studied local cluster, Coma is the zero-redshift baseline for many studies of high-redshift clusters (e.g. Jorgensen et al. 2006). Comparison between low- and high-redshift clusters is vital for our understanding of their evolution, which in turn is essential if we are to disentangle evolutionary effects from the properties which tell us about their formation.

We describe here the HST/ACS Coma Cluster Treasury survey, which aims to provide an unparalleled database of high spatial resolution images of a sample of cluster galaxies. At the distance of the Coma cluster ($\sim$100 Mpc), the resolution of HST/ACS ($0''.1$) corresponds to $\sim$50 pc. This gives essentially the same physical resolution as ground-based observations have in Virgo and Fornax. Thus the HST/ACS Coma database provides a valuable comparison between high- and low-density clusters, for studies of the effect of environment on galaxy components.

Whilst the HST observations are the prime data upon which this survey is based, it has already generated numerous ancillary observations with facilities such as Subaru, Keck, MMT, UKIRT. It is concurrent with surveys of the cluster in other wavebands, including the ultra-violet (GALEX), infra-red (SPITZER), X-ray (Chandra and XMM-Newton) and radio (VLA).

2. Scientific Motivation

2.1. The Luminosity Function

The logarithmic slope of the low-mass end of the Cold Dark Matter (ΛCDM) mass function has a slope $\alpha \approx -1.8$ (e.g. Somerville & Primack 1999). In contrast, the faint end of the field-galaxy luminosity function has a slope $\alpha \approx -1.3$, when measured either from optically-selected surveys (Blanton et al. 2005), or H I (Zwaan et al. 2005) or $\alpha \approx -1.0$, when measured in the K-band (Gardner et al. 1997; Kochanek et al. 2001). Luminosity functions in clusters and groups are often not well fit by a single Schechter function (Smith et al. 1997), and are better modeled by a combination of a Gaussian and a Schechter function (Ferguson & Sandage 1991). The composite behavior of the LF and the trends with cluster richness are beginning to be understood in the context of the conditional luminosity function (Cooray & Cen 2005), which provides a powerful conceptual framework for exploring the physics of galaxy formation via studies of halos (clusters and groups) of different mass. The suppression of the faint-end slope of the LF relative to the CDM mass function is widely believed to be due to photoionization by the meta-galactic UV background, which suppresses star-formation in low-mass halos. This predicts an environmental dependence (Tully et al. 2002) because the fraction of dwarf-mass subhalos that collapse before re-ionization is larger in higher mass halos, i.e., much larger in a $10^{14} M_{\odot}$ halo than in a $10^{11} M_{\odot}$ halo. This prediction can be tested directly with our survey, as the very faint-end of the LF slope in Coma should be closer to the CDM prediction, and at least some of the dwarfs should have very old stellar populations.

From earlier HST/WFPC2 data of a small area around NGC 4874 in the core of the Coma cluster, Milne et al. (2007) determine a steep faint-end slope ($\alpha \approx -2.0$), which agrees with the slope for the faintest objects in a small-area imaging study by Bernstein et al. (1995), but not with studies using spectroscopic redshifts (Mobasher et al. 2003).

Measurements of the faint-end LF slope in the Virgo cluster have been made by a number of authors, e.g. Trentham & Hodgkin (2002), and Sabatini et al. (2007). Trentham & Hodgkin (2002) find that the LF rises rapidly ($\alpha \approx -1.6$) between $M_B = -16$ and $M_B = -14$, but flattens faintward of this. The results of Sabatini et al. (2007) again suggest a steep slope between $M_B = -16$ and $M_B = -14$, flatter between $M_B = -14$ and $M_B = -11$. Trentham & Tully 2002 analyse the slope of the faint end of the LF in a number of lower density groups. They find a mean slope of $\alpha \approx -1.2$ over a large range from $M_B = -18$ to $M_B = -10$. Mieske et al. (2007) use SBF measurements to determine cluster membership in Fornax, and find an even flatter faint-end slope, similar to that in the local group ($\alpha \approx -1.1$). These authors point out however that the absolute number of dwarfs per unit virial mass is

higher in the lower density environments. Sabatini et al. (2007) concur that the luminosity function slope in the field is flatter than in the Virgo cluster, although they parameterise this in terms of a Dwarf to Giant Ratio (DGR). These studies present a consistent picture of a faint-end LF slope which is strongly dependent upon the density of the environment, and our study of the Coma LF, at a variety of galaxy densities, will present an important extension to this work.

The area of the survey reduces the vulnerability of determinations of the faint-end slope to poor statistics and cosmic variance (Driver et al. 1998), and provides a sufficient range of galaxy density to test variations in the faint-end LF across different cluster environments (e.g. Phillipps et al. 1998). The depth and spatial resolution allow the use of surface brightness and morphological criteria to assess the probability of cluster membership (Trentham et al. 2001; Trentham & Tully 2002) and examination of the relative contribution of dE, dS0 and dIrr galaxies to the faint end LF, and of the possible evolutionary relationship between these types (Aguerri et al. 2005; Mastropietro et al. 2005).

Different formation mechanisms give rise to the disk, bulge and bar components of galaxies. To understand the relative dominance of these physical processes in the Universe therefore requires one to construct not simply a galaxy luminosity function, but separate bulge, bar and disk luminosity functions (Driver et al. 2007a; Laurikainen et al. 2005). The dust-corrected Millenium Galaxy Catalogue (Driver et al. 2007b) provides a field galaxy comparison for the Coma component luminosity functions.

2.2. Structure and scaling laws of dwarf galaxies

Early-type galaxies exhibit well-defined empirical correlations between global galaxy parameters, such as luminosity, radius, surface brightness, color, velocity dispersion, and line strength indices (Kormendy 1985; Faber & Jackson 1976; Bender et al. 1992; Guzmán et al. 1993; Graham & Guzmán 2003). These scaling laws can tell us a great deal about the physical processes operating during galaxy formation, of which major contributors are star-formation feedback (Efstathiou 2000), tidal interactions (Duc et al. 2004), and interactions with the hot intergalactic medium (Babul & Rees 1992; Roberts et al. 2004; Tully et al. 2002).

Despite being the most numerous galaxy type in nearby clusters, dE/dS0 galaxies are among the most poorly studied due to their low surface brightness ($21< \mu_e <25$ V mag/arcsec^2). The scaling laws for dwarf ($M_v > -19$) ellipticals and spheroidals are somewhat controversial, it is unclear whether dwarfs form a family of galaxies distinct from giants

(Wirth & Gallagher 1984; Kormendy 1985; Caon et al. 1993), or a continuous sequence with them (Caldwell 1983; Graham & Guzmán 2003). The ACS survey will allow sophisticated parameterisation of the surface brightness profiles of galaxies to $V \sim 21$ ($M_V \sim -14$); and measurement of basic structural parameters such as half-light radius and Sérsic (1968) index to $V \sim 23$ ($M_V \sim -12$). Such limits are similar to those for measuring velocity dispersions and line strengths with large ground-based telescopes. Substantial samples from multi-object spectrographs on 4 metre class telescopes down to $B \sim 19$ already exist (see section 1).

The study of the scaling laws in various environments also provides the key observational reference needed to test specific predictions of current theoretical models of dwarf galaxy formation and evolution. For instance, the galaxy harassment model predicts that dE/dS0s in the highest-density cluster regions should have steeper light profiles, the fraction of nucleated dE/dS0s should be higher, the fraction of any remaining disk structure should be lower, and they should have higher metallicities than those located in lower-density cluster environments (Moore et al. 1998).

2.3. The effect of environment upon morphological components

The high density in the Coma cluster core makes it an ideal place to investigate the morphology-density relation, in which the average bulge-to-disk (B/D) luminosity ratio increases with galaxy density (Dressler 1980). This is understood to result from transformation of spirals into early types through processes such as harassment (Moore et al. 1996). An example of this transformation in progress may be the Coma cluster galaxy GMP 3629 (Graham, Jerjen, & Guzmán 2003). Furthermore, there is a strong radial gradient in HI content in the spirals, those in the cluster core being severely depleted (Bothun et al. 1984; Bravo-Alfaro et al. 2000). This, together with similar results in Virgo, supports the notion of gas stripping and the subsequent cessation of star formation (Conselice et al. 2003). From a quantitative morphological analysis using high-quality ground-based images, Gutierrez et al. (2004) find that disks in the Coma core are 30% smaller than in the field for a given bulge size.

Bulge-disk decomposition in the presence of nuclear components depends critically on spatial resolution (Balcells et al. 2003). The high resolution of ACS allows identification of disks, unobscured primary and nuclear bars, classical bulges, resonance starburst rings, compact disks, disky bulges, and pseudo-bulges (e.g., Kormendy & Kennicutt 2004; Athanassoula 2005). While observations in the rest-frame I-band (F814W) may miss some highly obscured morphological features, a comparison of the optical properties across field and dense clusters will set important constraints on how environment influences the morphology and structure

of galaxies. The radial dependence of bulge and disk morphologies can constrain the roles of mergers (Aguerri et al. 2001) and of disk truncation processes.

2.3.1. Stellar Bars and Disks

Stellar bars redistribute angular momentum in disk galaxies, driving their dynamical and secular evolution (Erwin et al. 2003; Kormendy & Kennicutt 2004; Jogee et al. 2004, 2005; Erwin 2005). Many barred galaxies host molecular gas concentrations of up to several thousand $M_{\odot}$ pc^{-2} in the inner kpc, intense circumnuclear starburst rings, and disky bulges (e.g., Jogee 1999; Jogee et al. 2005). Bars are abundant in the field out to $z \sim 1.0$, corresponding to the last 8 Gyr (Elmegreen et al. 2004; Jogee et al. 2004; Zheng et al. 2005), however we know much less about barred disks in dense clusters. Varela et al. (2004) note that bars are twice as frequent in perturbed galaxies as in isolated galaxies, and Elmegreen et al. (1990) note a higher frequency of bars in binary galaxy systems compared with isolated galaxies, so there is some evidence for variation with environment. The closest to a systematic environmental survey is that of van den Bergh (2002), who found the frequency of bars in spiral galaxies in clusters and in the field to be similar, although he did not probe the richest cluster environments.

Bars and similar structures (e.g., nuclear bars, rings, and spirals) are detectable in HST images if they have diameters $\sim$ 3–5 FWHM (Sheth et al. 2003; Jogee et al. 2004; Lisker et al. 2006). At the resolution of the Coma survey they will be detected down to sizes of $r \sim 150$ pc. This will enable identification and characterization of unobscured large-scale bars across the Hubble sequence (e.g., Erwin 2005), and across different environments. In moderately inclined galaxies, the survey can identify compact disks and disky "pseudobulges" (Erwin et al. 2003; Kormendy & Kennicutt 2004; Athanassoula 2005; Jogee et al. 2005). Coma is an excellent case study for the significance of inner/nuclear components in S0 and spiral galaxies, and a key reference for comparison with studies of nuclear bar and ring frequencies in local field samples (e.g. Erwin & Sparke 2002; Laine et al. 2002; Knapen 2005).

The surface brightness profiles of stellar disks fall into three classes (Erwin, Beckman, & Pohlen 2005; Pohlen & Trujillo 2006; Erwin, Pohlen, & Beckman 2007): classic single-exponential profiles, downward-bending "type II" profiles (Freeman 1970; "truncations"), and upward-bending "type III" profiles ("antitruncations"). Type II profiles are common in early-type barred galaxies, and appear linked to the Outer Lindblad Resonance of bars; type III profiles, on the other hand, appear anti-correlated with bars, and may be a signature of minor mergers (Younger et al. 2007). A comparison of barred S0–Sb galaxies in the Virgo Cluster and the local field shows a dramatic dichotomy: type II profiles are common in the

field but essentially absent in Virgo (Erwin 2007, in prep). If this can be confirmed for the Coma Cluster, it points to a clear role for the cluster environment in shaping the outer disks of S0's and early-type spirals, and suggests an important test for distinguishing models of S0 formation in clusters from the field.

2.4. Colour gradients and stellar populations

The steepness of the radial color gradients of dwarf and giant galaxies directly reflects their merging history: monolithic collapse imposes an initially steep negative metallicity gradient (Carlberg 1984), which will be progressively diluted by subsequent major mergers (Bekki & Shioya 1999; Kobayashi 2004). Semi-analytic models of hierarchical galaxy formation predict differences in the merger history as a function of galaxy mass and environment (Cole et al. 2000). The Coma survey provides an unbiased sample of cluster dwarfs, so that the global scaling relations of different dwarf subtypes (dE, dS0, dE-N, dIrr) can be reliably determined. Coma ellipticals have metallicities that seem to correlate with galaxy mass, which is broadly consistent with monolithic collapse models (e.g. Forbes et al. 2005). In contrast, dwarf ellipticals and spheroidals display a variety of color gradients, even positive in some places, which is an indication of recent star formation (van Zee et al. 2004).

Complemented by K-band and IFU observations, the ACS images can be used to interpret the observed color distributions in terms of ages and metallicities, using photometric techniques (James et al. 2006) and line indices (e.g. Poggianti et al. 2001; Mehlert et al. 2003; Sánchez-Blázquez et al. 2006).

2.5. Globular clusters and UCDs

The Coma cluster hosts several bright early-type galaxies, which are known to have very rich globular cluster (GC) systems (Ashman & Zepf 1998), and many less massive galaxies with their own star cluster systems that were assembled and evolved in the dense Coma cluster environment. There have been HST/WFPC2 studies of the GC systems of a small number of bright Coma ellipticals: IC 4051 (Baum et al. 1997; Woodworth & Harris 2000), NGC 4881 (Baum et al. 1995) and the cD galaxy NGC 4874 (Kavelaars et al. 2000; Harris et al. 2000). Marín-Franch & Aparicio (2002) find a wide range of specific frequency S_N values among the brighter galaxies in Coma, using the Surface Brightness Fluctuation (SBF) technique on ground-based data.

The ACS Virgo cluster survey has provided a number of important new results on the

GC populations of early-type galaxies in the sparser Virgo cluster (e.g. Jordán et al. 2005; Peng et al. 2006a; Mieske et al. 2006). At the distance of Coma it is only possible to resolve half-light radii down to $\sim$20 pc ($0''.04$). Moreover, the peak of the Globular Cluster Luminosity Function (GCLF) in Coma is suspected to be at $V = 27.88 \pm 0.12$ (Kavelaars et al. 2000), some 1.3 magnitudes fainter than our 10-σ photometric completeness limit for point sources. Nevertheless, if the GCLF has a Gaussian form with $\sigma = 1.4$ magnitudes some 18% of the GCs are expected to be brighter than this limit, allowing us to study the color distributions, color-magnitude diagrams and spatial distribution of GCs in a much wider range of galaxies than in the targeted Virgo cluster survey (from M_V = -23.3 to -15), to a larger physical radius from the galaxy centers (up to 100 Kpc). Stacking the GC systems of galaxies in bins will allow study of their properties as a function of host galaxy type, luminosity and environment, and thus of the relationship between GC systems and their hosts, and the processes which lead to the formation of the rich GC systems of the massive galaxies (Pipino et. al. 2007)

2.5.1. The spatial distribution of clusters and the epoch of reionization

The old, metal-poor GC population in giant ellipticals may provide the best available tracer of their dark halos, and thus may be useful in testing the predictions of ΛCDM models. Moore et al. (2006) and Bekki & Yahagi (2006) find that the final radial distibution of the old GCs depends upon the redshift of truncation of GC formation, which in turn might depend upon the epoch of reinonization. If the truncation is earlier, then the final radial GC distributions will be steeper and more compact (Bekki & Yahagi 2006).

Bassino et al. (2006) present a study of the globular clusters around NGC 1399, the dominant galaxy in the Fornax cluster. They note a good agreement with a projected dark matter NFW (Navarro et al. 1996) density profile. Abadi et al. (2006) test the radial density profile of GCs around the somewhat isolated galaxies M31 and the Milky Way, comparing with the numerical simulations. They report that such luminous halos are similar in shape to their dark matter counterparts. On the other hand Merritt et al. (2006) in a careful analysis of a set of ΛCDM simulations, find that the halo density distributions are better fit by the much earlier model of Einasto (1965, 1972, 1974) than by NFW or a number of other alternative models.

2.5.2. UCDs and transition objects

Ultra-compact dwarfs (UCDs), at $-13.5 \leq M_V \leq -11.5$, have been detected from the ground in the Fornax and Virgo Clusters (Hilker et al. 1999; Drinkwater et al. 2000; Phillipps et al. 2001; Jones et al. 2006). HST imaging of the bright Fornax UCDs shows that they have half-light radii of $10-20$ pc, larger than both Local Group GCs and typical dwarf galaxy nuclei, but smaller than any previously known dwarf galaxies (De Propris et al. 2005). Similar but fainter objects have since been found (Haşegan et al. 2005 - their dwarf galaxy globular cluster transition objects, DGTOs). These overlap in luminosity with, the brightest GCs, leading to the question of whether UCDs and large GCs are indeed fundamentally different objects. UCDs and DGTOs appear to be a feature of denser environments, so it is important to quantify the population of this new type of object in Coma and compare it with the less rich Virgo and Fornax.

Proposed scenarios see UCDs (see Hilker 2006, for a review) as the tidally 'threshed' remnant nuclei of former nucleated dwarf elliptical galaxies in the cluster core (Bekki et al. 2001), the similar remains of late-type spirals with nuclear star clusters (Moore et al. 1998), more massive, perhaps intra-cluster versions of ordinary GCs (Hilker et al. 2004), merged (super)star clusters (Fellhauer & Kroupa 2002), products of massive starbursts during the merger of two gas-rich galaxies (Fellhauer & Kroupa 2005), or even left-over primordial building blocks of central galaxies in the dense galaxy cluster environment (Rakos & Schombert 2004).

The point source magnitude limit of the Coma survey is deep enough to observe compact objects down to $M_V \simeq -9$ mag, so we can detect both UCDs and DGTOs down to GC luminosities. At the distance of Coma, the half-light radii of the brighter examples will be 0.02 to 0.04 arcsec, corresponding to $\sim 10 - 20$ pc (Drinkwater et al. 2003). These sizes are similar to those of extended star clusters in the Virgo Cluster which have been successfully differentiated from point sources by Peng et al. (2006b) using ACS. They can be reliably distinguished from background galaxies at magnitudes $V \sim 22$ to 25 mag which have half-light radii typically between 0.2 and 1.0 arcsec (e.g. Roche et al. 1997).

2.6. The nature of "E+A" galaxies

Spectroscopic surveys (Caldwell et al. 1993; Poggianti et al. 2004) have identified several galaxies with post-starburst spectra in both the core and the infall region of Coma. Suggestions as to what triggered these bursts range from equal-mass galaxy mergers (Barnes & Hernquist 1992) to high-speed impact with shock fronts of infalling substructures (Poggianti

et al. 2004) or generally with the dense ICM (Tran et al. 2005). The key to distinguishing between these processes is the spatial distribution of the intermediate-age populations. It would be concentrated to the center if major mergers were involved (Barnes & Hernquist 1992) while it would be either an extended or off-centered phenomenon if the galaxy had experienced an interaction with the ICM. The Coma survey includes a number of "E+A" or "k+a" galaxies at a range of luminosity, and the morphological features and color maps generated from the two ACS passbands will provide a valuable diagnostic of the physical origin of the "E+A" phenomenon.

2.7. Nuclear Star Clusters and Central Massive Objects

Massive black holes at the centers of spheroidal stellar systems correlate with the large scale properties of the host spheroid. Popular correlations involve: (i) spheroid velocity dispersion (Ferrarese & Merritt 2000; Gebhardt et al. 2000); (ii) stellar concentration (Graham et al. 2001; Graham & Driver 2007); (iii) luminosity (McLure & Dunlop 2002; Marconi & Hunt 2003; Graham 2007); and (iv) mass (Marconi & Hunt 2003; Häring & Rix 2004).

The relationship between nuclear star clusters and central massive objects is of increasing interest, although the formation of the former remains poorly understood. They are observed in about 80% of intermediate-luminosity, early-type galaxies (e.g., Ferguson & Binggeli 1994; Graham & Guzmán 2003; Coté et al. 2006; Jordan et al. 2007; Balcells et al. 2007). Graham & Guzmán (2003) find that the luminosity of nuclear star clusters in dEs correlates strongly with the luminosity of the host spheroid. This luminosity trend has also been shown to exist in the bulges of lenticular and early-type spiral galaxies (Balcells et al. 2003). It has also been proposed that they follow the same $M_{\rm nucleus}$–$M_{\rm spheroid}$ relation as defined by supermassive black holes (Ferrarese et al. 2006b; Balcells, Graham & Peletier 2007), and the same $M_{\rm nucleus}$–Sersic index relation (Graham & Driver 2007).

Graham & Driver (2007) suggest that the driving physical relation may be with the central stellar density (prior to core depletion) rather than a *global* property of the host spheroid. Given the known trend between central stellar density and host spheroid luminosity (e.g., Graham & Guzmán 2003; Merritt 2006a), the relations with global properties may be secondary in nature. It is therefore important to examine the connection between the mass of the nuclear star clusters and the central stellar density (projected, μ_o, and deprojected, ρ_0) of the host spheroid.

Study of the luminosity function, color-magnitude relation, relationship between nuclear and host galaxy color, and the radial distribution within the cluster (Ferguson & Sandage

1989; Lisker et al. 2007), and comparison with the lower density Fornax and Virgo environments, may help shed some light on potential formation mechanisms. Measurement of spatial offsets between nuclear clusters and the outer isophotes may reveal an oscillation of the nucleus about the center of the potential, which will be of larger amplitude in shallower potentials (Binggeli et al. 2000). Furthermore, apparant double nuclei may in some cases be a sign of an edge-on nuclear disk (Kormendy 1988; Tremaine 1995), from which we may be able to determine the presence of a central massive black hole (e.g. Debattista et al. 2006).

Giant elliptical galaxies display cores which are partially depleted of stars. A possible mechanism is the wrecking ball action of supermassive black holes (SMBHs) from the progenitor galaxies as they sink to the center of the newly-formed galaxy during a merger (Begelman et al. 1980; Ebisuzaki et al. 1991, Merritt et al. 2007). Cores may also be enlarged when black holes are ejected from galaxy centers by the gravitational wave rocket effect following coalescence of a SMBH binary (Redmount & Rees 1989; Merritt et al. 2004; Gualandris & Merritt 2007).

Using the core-Sérsic model (Graham et al. 2003; Trujillo et al. 2004) it is possible to quantify the sizes (and mass deficits, $M_{\rm def}$) of these cores, and to predict each galaxy's central black hole mass, $M_{\rm bh}$, using the measured Sérsic index n (e.g., Graham & Driver 2007). Given that $M_{\rm def}/M_{\rm bh}$ scales roughly linearly with N, where N is the number of major dry mergers, such measurements can be used to place constraints on the dry merger history of such cluster galaxies (Graham 2004; Ferrarese et al. 2006a; Merritt 2006b), and to constrain N as a function of galaxy magnitude.

3. Survey Design

3.1. Survey area

The ACS Wide Field Camera (ACS/WFC) has a field of view of 11.3 square arcminutes. The camera contains two 4096 x 2048 pixel CCDs, with an inter-chip gap of some 3 arcseconds. The capabilities of ACS at the time of our pre-anomaly observations are descrived in some detail by Pavlovsky et al. (2006).

The aim of the survey is to provide a large sample of galaxies for study in a high density environment, and at the same time a comparison sample in a lower density region of the cluster for the specific science goals of examining the effect of environment upon morphology, structural parameters and stellar populations. Because of the density of confirmed cluster galaxies in the core (e.g. Colless & Dunn 1996) we have adopted a tiling strategy in the core region, tiling a region of approximately 18 x 21 arcminutes, using 42 ACS pointings in a 7

x 6 pattern, with some overlap between adjacent tiles. An HST orientation of 282 degrees was chosen for these tiles in order to maximise the time for which the obeservations could be scheduled in two gyro mode (Sembach et al. 2006). A tile of the central mosaic was moved to the southern edge of the mosaic area, away from the star HD112877 (V=7.17) which would have a negative impact on ACS observations near its position.

In the outer part of the cluster the density of known members is less than one per ACS tile, and we decided to target known members which can be used to address some of our primary science goals. The best studied region outside the core is the infall region around NGC4839 (Neumann et al. 2001) where there have been a number of photometric surveys (Komiyama et al. 2002) and spectroscopic surveys for poststarburst galaxies (Caldwell et al. 1993), and line strengths and velocity dispersions of dwarf spheroidals (Poggianti et al. 2001; Matkovic & Guzmán 2005, 2008; Cody et al. 2007). 40 further ACS pointings were defined, each containing one, or in most cases more, cluster members from these spectroscopic surveys. In some cases the orientation was left free in the HST Phase 2 submission, in others a range was defined in order to ensure that more than one target galaxy was included. Table 6 lists the positions and orientations of our survey tiles. In this Table Column 1 gives the HST Visit number within the program; column 2 the field title. Columns 3 and 4 give the field center RA and Dec, and column 5 the field orientation of the observation, or the orientation specified for visits which have not yet been completed. Column 6 lists the spectroscopically confirmed cluster members within the field, with identifiers: GMP from Godwin et al. (1983); K from Komiyama et al. (2002). Column 7 gives the date of the observation, and column 8 the number of dither positions which have been observed by the time of the January 2007 ACS failure. At this time, 21 of our 82 fields have been fully observed, and further 4 have either two or three dither positions observed. The survey is thus 28% complete.

Figure 2 shows in the left panel the positions and orientations of the survey tiles, and the locations of NICMOS parallel observations. For cases where a range of orientations are specified in the Phase 2 submission the orientation shown is the midpoint of the range, and those tiles with free orientation are shown at 90 °. The positions and final orientations of the 25 fully or partially observed fields are shown in the right hand panel of this figure.

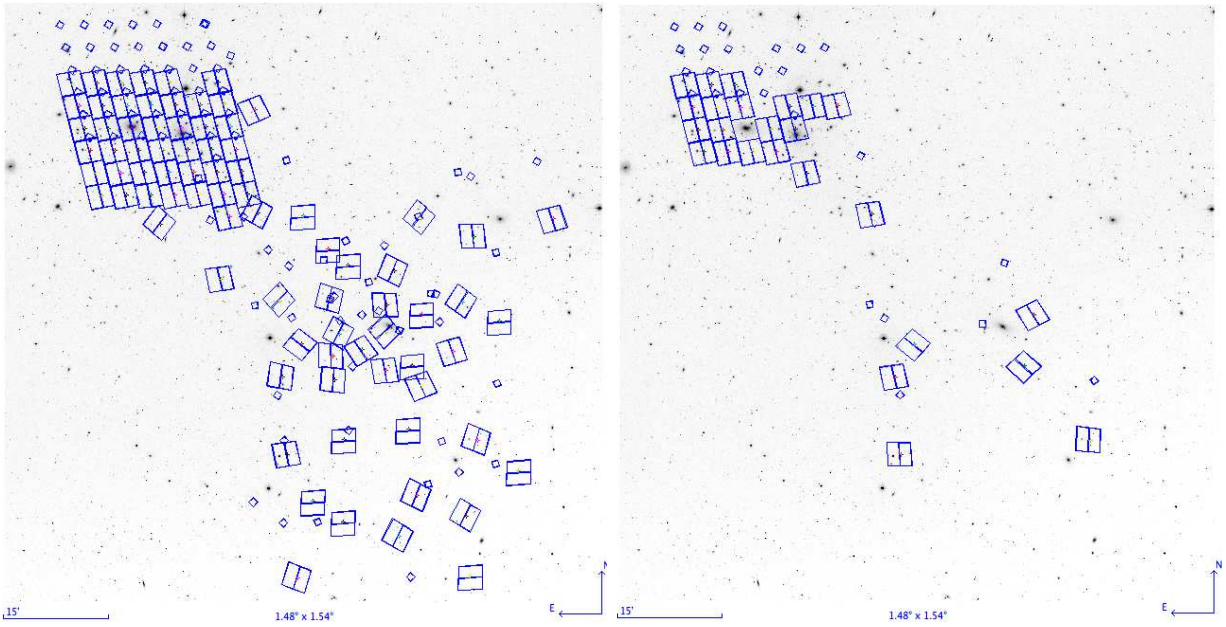

Fig. 2.— Left: Positions of ACS tiles for the survey proposed, overlayed on a DSS image of the core and infall region of the Coma cluster. The small squares represent the fields of NICMOS parallel exposures. Right: The survey as at the ACS failure of January 2007. Tiles shown have some or all of the proposed observations complete by this date.In this panel requested orientations are replaced by observed orientations if they differ.

3.2. Choice of passbands, exposure times and dither parameters

Color information is essential to some of the most important aims of the survey, so we require two passbands. For these passbands we choose F814W, as the passband which will give the deepest data for structural and luminosity function studies, and F475W, which is a compromise between color baseline and speed. These passbands are close to Cousins I and SDSS g' respectively. Transformations from these ACS/WFC passbands to standard Johnson/Cousins passbands are given by Sirianni et al. (2005). Total system throughput as a function of wavelength for all ACS/WFC filters, from the work of Sirianni et al. (2005), is given on the ACS project website [1] and we plot in Figure 3 the throughput for our two passbands.

[1]http://adcam.pha.jhu.edu/instrument/photometry/

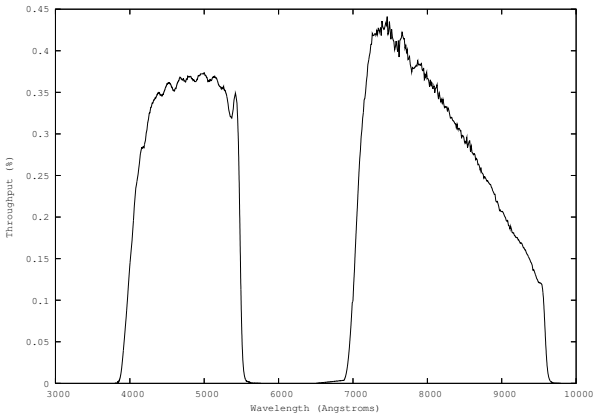

Fig. 3.— Total throughput curves of ACS CCDs plus filter for F475W passband (left) and F814W passband (right), after Sirianni et al. (2005)

We defined a dithering pattern with a large (3 arcsecond) dither across the inter-CCD gap on ACS/WFC, plus a sub-dither to remove hot pixels, resulting in four positions over the two orbits. The large move was made between orbits. Each passband was observed at each dither position. The large dither point spacing was 3.011 arcseconds at a pattern orientation of 85.28°, and the hot pixel sub-dither spacing was 0.2412 arcseconds at a pattern orientation of 22.3239°. POS-TARG equivalent positions are given in Table 2.

Table 2. POS-TARG equivalent of dither pattern used

Dither Position	POS-TARG	
1	0.0	0.0
2	0.222	0.092
3	0.247	3.001
4	0.469	3.093

Exposure times were 350 seconds in F814W and 640 seconds in F475W at each dither position. F814W frames are somewhat deeper than F475W, but it was not possible to distribute the time more towards F475W, as this would have resulted in F814W frames too short to dump the ACS buffer, and thus a substantial increase in overheads. In some visits the F475W exposure time for the final dither position could be slightly longer, due to savings in the reacquisition overhead (as compared with the original acquisition), resulting in a total F475W integration time of between 2560 and 2680 seconds.

In Table 3 we present magnitudes and surface brightnesses for signal-to-noise ratio (S/N) = 10, calculated with the ACS Exposure Time Calculator (ETC). In these calculations the ETC is set to assume standard background conditions, and an elliptical galaxy spectral energy distribution. The ETC gives two values for S/N for a point source: that in the "default" aperture, which for ACS/WFC is a circle of 0.2 arcsec radius; and an "optimal" S/N, assuming that a PSF fitting algorithm is used. In columns 3 and 4 of Table 3 limits are presented in each passband for each of these S/N values to reach 10.

The real completeness and reliability limits, and contamination with spurious sources near these magnitude limits will depend upon real background conditions, to which the halos of large galaxies will contribute, and upon real HST guiding performance. For point sources we have estimated the limits by injecting artificial point sources into our ACS frames from one of our outer fields, and recovering them with SExtractor. In column 5 of Table 3 we present the magnitude at which 90% of artificial injected sources are recovered. This limit is, as expected, between the two calculated limits, but encouragingly close to the "optimal S/N" calculated limits.

For galaxies the limits will depend upon surface brightness and structural parameters. These will be discussed further in Paper II in this series (Hammer et al. 2008).

In column 6 of Table 3 we present a calculated limit in mag arcsec^{-2}, obtained (using the ETC) for a S/N = 10 for a uniform surface brightness region of 1 arcsec^2.

All magnitudes and surface brightnesses have been converted from the Vega magnitude system used by the ETC to AB magnitudes, using the AB magnitude of Vega in the chosen filters (e.g. Sirianni et al. 2005).

Table 3. Columns 3 and 4 - predicted 10σ limits for optimal extraction of point sources; column 5 - limit for 90% recovery of injected point sources; column 6 predicted surface brightness (1 sq arcsec) limits; all in the AB magnitude system.

Passband	Exposure (seconds)	ETC Limit (S/N=10) "Default"	ETC Limit (S/N=10) "Optimal"	Measured 90% recovery	SB (mag arcsec^{-2}) S/N=10 in 1 arcsec^2
F475W	2560	$g' = 26.75$	$g' = 27.6$	$g' = 27.55$	$g' = 25.8$
F814W	1400	$I_C = 25.95$	$I_C = 26.8$	$I_C = 26.65$	$I_C = 25.0$

4. ACS Data Reduction

The ACS data processing was performed at STScI. It involved a dedicated pipeline based on a wrapper script using PyRAF/STSDAS modules that performed CCD data reduction and cosmic ray cleaning, as well as the combination of individual dithered images using `MultiDrizzle` (Koekemoer et al. 2003), which makes use of the `Drizzle` software (Fruchter & Hook 2002) to remove geometric distortion and map the input exposures onto a rectified output frame. We describe details of the ACS data reduction below.

4.1. Initial CCD Reduction

As the observations of each *HST* visit were obtained, the data were run through the STScI on-the-fly-reprocessing (OTFR) pipeline for ACS data. This pipeline reduction involves basic CCD reduction by means of the IRAF/STSDAS task `calacs`, which performs bias subtraction, gain correction, dark subtraction, flat fielding, and the identification of bad pixels. Finally, the OTFR pipeline identifies the exposures taken through each filter (F475W vs. F814W) and combines them using the OTFR version of `MultiDrizzle` for ACS data. These first-pass pipeline products were used for quicklook purposes. Final images were created by a second-pass calibration procedure which contained the steps described below.

4.2. Updated Reference Files

A few weeks after the each visit's data were observed, we downloaded more accurate calibration reference files from the *HST* archive, in particular the up-to-date superbias and superdark reference files which were created from bias and dark exposures obtained contemporaneously with the science data (see, e.g., Lucas et al. 2006). These files were used for the final calibrations.

4.3. Bias Level Offsets

In virtually all ACS datasets of our Coma survey, we encountered significant bias level offsets between the four quadrants of the `MultiDrizzle` output images. These offsets, which ranged from a few tenths to several Data Numbers, are due to randomly varying differences between the bias level in the parallel overscan region of a given ACS/WFC CCD chip and the level in its active region (see, e.g., Sirianni et al. 2003; note that ACS/WFC contains four

CCDs that are read out by their own amplifiers). A script was developed to measure these bias offsets between the four quadrants using iterative statistics on a large number of pairs of areas located close to (and symmetrically relative to) the quadrant-to-quadrant borders. The measured offsets were subtracted from the appropriate quadrants of the superbias reference file being used in the final image reduction of each set of exposures with a given filter.

4.4. Image Registration

In many cases, the spatial registration of images taken during each *HST* visit of this Coma treasury program was less accurate than expected, even though all images were planned to be taken without any change of prime guide star, telescope position or roll angle. This problem was due to two compounding circumstances: *(i)* several visits were forced to use single-star guiding due to unforeseen problems with the *HST* Guide Star Catalog version 2 in the region of the Coma cluster, *(ii)* the observations of our program unearthed a software bug in the ground system of the two-gyro guiding mode of *HST* for guide star reacquisitions when single guide stars were used. The result of these issues was that significant spatial offsets are present between images (and their world coordinate system (WCS) header keywords) taken in different *HST* orbits, even if taken during one and the same visit. Since it is crucial to align images to better than $\sim 5-8$ milliarcseconds (i.e., $\lesssim 0.15$ ACS/WFC pixel) in order to achieve accurate cosmic ray rejection among the separate exposures within a visit and to retain satisfactory point spread functions (PSFs) in the combined image, we registered all images within a visit to a common astrometric grid as follows.

First, we ran `MultiDrizzle` on every set of associated images (i.e., images taken in one visit with the same filter) using the `driz_separate = yes` setting. This created so-called "singly drizzled" images, which are the individual input science images in the same format as the default output files from `MultiDrizzle`, i.e., after correction for geometric distortion using the WCS keywords in the image header. SExtractor (Bertin & Arnouts 1996) was then run with a signal-to-noise threshold of S/N = 10 on each single drizzled image. The resultant catalogs were trimmed on the basis of object size and shape parameters, thereby rejecting the vast majority of cosmic rays, CCD artifacts, and diffuse extended objects. Further catalog trimming was done by visual inspection of the 2-dimensional structure of the catalog sources, only retaining compact sources (non-saturated stars and compact galaxies). Typically, 3 – 15 "good" sources remained available for proper image alignment. Using these object catalogs, residual shifts (called 'delta shifts' in `MultiDrizzle` nomenclature) and rotations ($\Delta x,\ \Delta y,\ \Delta\theta$) between the individual singly drizzled images and a reference image were determined using IRAF tasks `xyxymatch` and `geomap`. The reference image was always

taken to be the image observed first in the visit. The resulting delta shifts and rotations were then fed to a second run of `MultiDrizzle` using `driz_separate = yes` to verify the result of the alignment. This often prompted the need for a second iteration of the alignment process. The formal uncertainties of the alignment process stayed below 0.1 ACS/WFC pixel (as reported by the `geomap` task).

4.5. Cosmic Ray Rejection

Once the alignments between the individual images were determined, cosmic ray rejection was done nominally in two steps. The first step was performed by using `MultiDrizzle` and its cosmic ray rejection algorithm, which uses a process involving an image containing the median values of each pixel in the (geometrically corrected and aligned) input images as well as its derivative (in which the value of each pixel represents the largest gradient from the value of that pixel to those of its direct neighbors; this image is used to avoid clipping bright point sources) to simulate a "clean" version of the final output image. For a typical 640-second F475W exposure, $\sim 100,000 - 320,000$ pixels were affected by cosmic ray hits, i.e., $\sim 0.6 - -2\%$ of the 4096^2 pixels. Thus, it is exceedingly rare for a pixel to be affected by cosmic rays during all four exposures (namely ≤ 3 pixels out of 4096^2). The number of pixels affected by 3 cosmic rays out of 4 exposures was however significantly higher (up to ~ 120 pixels). In the latter cases, the median value was replaced by the value of the one valid pixel if the median value was larger than that of the valid pixel by a 5σ threshold. This process yielded satisfactory results for the bulk of the tiles, except for the central strip of pixels in each tile which only had contributions from two exposures due to the gap between the two CCD chips of ACS/WFC. Furthermore, the `MultiDrizzle` output images of the tiles which only had two or three successful exposures also contained several residual pixels affected by cosmic rays. For the central strips in the tiles with four exposures and the full tiles with only two or three exposures, we therefore used a second step of cosmic ray rejection by means of the `lacosmic` routine (van Dokkum 2001) using parameter values chosen after careful testing.

4.6. Construction of Final ACS Images

Before the final run of `MultiDrizzle` on the input images to produce the final image tiles using the cosmic ray masks created as mentioned in the previous subsection, we created sky variance maps for each individual exposure for the purpose of deriving appropriate weight maps for the final image combination. These maps contain all components of noise

in the images, except for the Poisson noise associated with the sources on the image. These maps were constructed from the sky values determined by MultiDrizzle for each individual exposure, the flatfield reference file, the dark current reference file, and the read-out noise values as listed in the image headers for each individual image quadrant (or read-out amplifier). These sky variance images were then inverted and used as weight maps for the associated exposures.

The final run of `MultiDrizzle` was performed by shrinking the input pixels by a factor 0.8 at the stage when the PSF is convolved by the input pixel scale (i.e., the `final_pixfrac` parameter). This factor was arrived at after some experimentation with different values, and was a good match to the degree of subsampling induced by the dither pattern we used. The final output images were produced in the default unrotated frame of the ACS/WFC CCDs rather than with North up so as to facilitate further analysis with PSF matching procedures.

5. NICMOS parallel observations

NICMOS parallel observations are made with the NIC3 camera of NICMOS in the J and H bands. The scientific motivations for these parallel observations, apart from that they are free, are the investigation of the near-IR luminosity function (LF), to compare with the SPITZER LF of Jenkins et al. (2007); a study of intra-cluster GCs, where the combined ACS (g,I) and NICMOS (J,H) data can be used to separate intermediate-age GCs from old halo globulars (e.g., Puzia et al. 2002); and a study of the near-IR fundamental plane for dwarf galaxies, where the relative insensitivity of the IR luminosity to dust extinction reduces the scatter in in the FP.

The NIC3 camera has a field of view of 51.2 arcsc square, with the 3 arcsecond dither to accomodate the ACS inter-CCD gap, the uniformly exposed area is approximately 48 x 51 arcsec per visit. The NIC3 field centre is some 8.5 arcminutes from the ACS field centre, at a position angle which depends upon the telescope orentation. The NICMOS fields are thus fairly random positions in the cluster, and as can be seen from Figure 2 only four of them overlap the area observed with ACS before the instrument failure. NICMOS parallel observations were taken on all pre-SM4 visits, of which 21 have the full four dither positions, these are summarised in Table 4.

Table 4. NICMOS parallel observations - field centres and exposures

Visit	RA	Dec	Exposure per filter (s)
1	13:00:53.82	28:13:10.9	2560
2	13:00:38.21	28:13:10.9	2560
3	13:00:22.61	28:13:11.0	1280
8	13:00:50.20	28:09:59.8	2560
9	13:00:34.61	28:09:59.9	2560
10	13:00:19.02	28:09:59.9	2560
12	12:59:47.81	28:09:59.8	1920
13	12:59:32.21	28:09:59.8	1280
14	12:59:16.61	28:09:59.9	1920
15	13:00:46.60	28:06:48.8	2560
16	13:00:31.01	28:06:48.9	2560
18	12:59:59.80	28:06:48.8	2560
19	12:59:44.21	28:06:49.9	2560
22	13:00:43.11	28:03:38.0	2560
23	13:00:27.40	28:03:38.0	2560
24	13:00:11.91	28:03:38.0	2560
25	12:59:56.31	28:03:38.0	2560
33	12:59:37.00	28:00:27.0	2560
45	12:58:49.90	27:33:21.2	2560
46	12:58:40.56	27:31:19.1	2560
55	12:57:22.73	27:38:58.6	2560
59	12:58:31.11	27:20:26.4	2560
63	12:56:26.40	27:21:58.4	2560
75	12:58:54.33	27:54:33.0	2560
78	12:57:37.50	27:30:20.6	2560

In 2560 seconds exposure per filter the calculated 10σ magnitude limits for optimal extraction of point sources in the AB magnitude system are J = 25.9 and H = 25.4.

6. Data and Educational products

Data products will include image data as processed by the ACS pipeline described above, and also object catalogs with a variety of structural parameters as described in Paper II and subsequent papers in this series.

The calibrated ACS images produced by STScI have been ingested into Astro-WISE[2](Valentijn et al 2006, Valentijn & Verdoes Kleijn 2006). Astro-WISE connects the distributed research groups for the data analysis and is used to create the source catalogs for the ACS images and to model the surface brightness distributions of galaxies. The results will be publicly available via the Astro-WISE web services.

ACS data will be associated in Astro-WISE with all COMA Legacy Survey products including derived products and ancilliary data (e.g. Subaru, INT and UKIRT imaging and multi-wavelength data). Astro-WISE also connects the survey to the EURO-VO.

Coma Legacy Survey data products will also be made available as part of the MAST Treasury archive at STScI[3]. Expected timescales for the distribution of data products are given in Table 5.

An education and public outreach (EPO) program has been designed whose goal is to share the valuable legacy dataset and the associated research with the public. The deliverables include:

1. *HST* ACS images of Coma that will appear at StarDate Online Astronomy Picture of the Week; in ViewSpace, which is seen in museums across the country; and in the revised StarDate/Universo Teacher Guide;

2. An activity and DVD targeted at 9th-12th grade students; and revised Internet versions of the StarDate/Universo Teacher Guide, which will highlight research on the Coma Cluster from *HST* data.

3. Five Stardate radio programs on the Coma Cluster in English, Spanish and German for

[2]http://www.astro-wise.org/

[3]http://archive.stsci.edu/hst/tall.html

distribution on monthly compact disk to over 500 radio stations in the USA, Mexico and Germany.

The EPO program is a coordinated effort between NASA, the University of Texas at Austin, the McDonald Observatory Education and Outreach Office, and the Space Telescope Science Institute (STScI)

Table 5. HST Data Products and Data Release Schedule

Data Product	Description	Release date
Raw Data	HST pipeline calibrated images	Immediate
Public catalog	Positions, magnitudes, geometry, color, from SExtractor	May 2008
Processed Image Data	Co-added, CR-cleaned, with best reference files	December 2008
Structural catalog	Multi-component structural analysis	December 2008
External data	Redshifts and ground-based colors	May 2009

This research and EPO program are supported by STScI through grants HST-GO-10861 and HST-E0-10861.35-A. We acknowledge Tony Roman and Marco Chiaberge at STScI for their technical help. S.J. acknowledges support from the National Aeronautics and Space Administration (NASA) LTSA grant NAG5-13063, and NSF grant AST-0607748. AWG is grateful for a Swinburne University of Technology RDS grant. THP gratefully acknowledges support in form of a Plaskett Fellowship atthe Herzberg Institute of Astrophysics. PE was supported by Deutsche Forschungsgemeinschaft Priority Program 1177. RJS is supported under the STFC rolling grant PP/C501568/1 "Extragalactic Astronomy and Cosmology at Durham 2005–2010". R.G. acknowledges additional support from the NASA LTSA grant NAG5-11635. BWM is supported by the Gemini Observatory, which is operated by the Association of Universities for Research in Astronomy, Inc., on behalf of the international Gemini partnership of Argentina, Australia, Brazil, Canada, Chile, the United Kingdom, and the United States of America. We thank the anonymous referee for very helpful comments.

REFERENCES

Abadi, M.G., Navarro, J.F., & Steinmetz, M. 2006, MNRAS, 365, 747

Adami, C. et al. 2006, A&A, 451, 1159

Adelman-McCarthy, J.K. et al. 2007, ApJS, in press.

Aguerri, J.A.L., Balcells, M. & Peletier, R.F. 2001, A&A, 367, 428

Aguerri, J.A.L., Iglesias-Páramo, J., Vílchez, J.M., Muñoz-Tuñón, C. & Sánchez-Janssen, R. 2005, AJ, 130, 475

Ashman, K. M., & Zepf, S. E. 1998, Globular cluster systems, Cambridge University Press

Athanassoula, E. 2005 MNRAS, 358, 1477

Babul, A. & Rees, M.J. 1992, MNRAS, 255, 346

Bai L., Rieke, G.H., Rieke, M.J., Hinz, J.L., Kelly, D.M. & Blaylock, M. 2006, ApJ, 639, 827

Balcells, M., Graham, A.W., Domínguez-Palmero, L. & Peletier, R.F. 2003, ApJ, 582, L79

Balcells, M., Graham, A.W., & Peletier, R.F. 2007, ApJ, in press

Barnes, J. & Hernquist, L. 1992, ARA&A, 30, 705

Bassino, L.P., Faifer, F.R., Forte, J.C., Dirsch, B., Richtler, T., Geisler, D. & Schuberth, Y. 2006, A&A, 451, 789

Baum, W.A. et al. 1995, AJ, 110, 2537

Baum, W.A., Hammergren, M., Thomsen, B., Groth, E.J., Faber, S.M., Grillmair, C.J. & Ajhar, E.A. 1997, AJ, 113, 1483

Begelman, M.C., Blandford, R.D., & Rees, M.J. 1980, Nature, 287, 307

Bekki, K., & Shioya, Y. 1999, ApJ, 513, 108

Bekki, K., Couch, W.J., & Drinkwater, M. 2001, ApJ, 552, L105

Bekki, K. & Yahagi, H. 2006, MNRAS, 372, 1019

Bender, R., Burstein, D. & Faber, S.M. 1992, ApJ399, 462

Bernstein, G.M., Nichol, R.C., Tyson, J.A., Ulmer, M.P. & Wittman, D. 1995, AJ, 110, 1507

Bertin, E. & Arnouts, S. 1996, A&AS, 117, 393

Binggeli, B., Barazza, F., & Jerjen, H. 2000, A&A, 359, 447

Blanton, M.R., Lupton, R.H., Schlegel, D.J., Strauss, M.A., Brinkmann, J., Fukugita, M. & Loveday, J. 2005, ApJ, 631, 208

Bonamente, M., Joy, M.K. & Lieu, R. 2003, ApJ585, 722.

Bothun, G.D., Schommer, R.A. & Sullivan, W.T. 1984, AJ, 89, 466

Bower, R.G., Lucey, J.R. & Ellis, R.S. 1992a, MNRAS, 254, 589

Bower, R.G., Lucey, J.R. & Ellis, R.S. 1992b, MNRAS, 254, 601

Bowyer, S., Korpela, E.J., Lampton, M. & Jones, T.W. 2004, ApJ605, 168

Bravo-Alfuro, H., Cayatte, V., van Gorkom, J.H. & Balkowski, C. 2000, AJ, 119, 580

Bravo-Alfuro, H., Cayatte, V., van Gorkom, J.H. & Balkowski, C. 2001, A&A, 379, 347

Briel, U.G., et al. 2001, A&A, 365, L60

Butcher, H., & Oemler, A., Jr. 1984, ApJ, 285, 426

Caldwell, N. 1983, AJ, 88, 804

Caldwell, N., Rose, J.A., Sharples, R.M., Ellis, R.S. & Bower, R.G. 1993, AJ, 106, 473

Carlberg, R.G. 1984, ApJ, 286, 416

Caon, N., Capaccioli, M. & D'Onofrio, M. 1993, MNRAS, 265, 1013

Cody, A.M., Carter, D. Bridges, T.J., Mobasher, B. & Poggianti, B.M. 2007, MNRAS, submitted.

Cole, S., Lacey, C.G., Baugh, C.M., & Frenk, C.S. 2000, MNRAS, 319, 168

Colless, M. & Dunn, A.M. 1996, ApJ458, 435

Conselice, C. J., O'Neil, K., Gallagher, J. S., & Wyse, R. F. G. 2003, ApJ, 591, 167

Cooray, A. & Cen, R. 2005, ApJ, 633, L69

Coté, P., et al. 2006, ApJS, 165, 57

Debattista, V.P., Ferreras, I., Pasquali, A., Seth, A., De Rijcke, S. & Morelli, L. 2006, ApJ, 651, L97

De Propris, R., Phillipps, S., Drinkwater, M.J., Gregg, M.D., Jones, J.B., Evstigneeva, E. & Bekki, K. 2005, ApJ, 623, 105

Dressler, A.R. 1980, ApJ, 236, 351

Drinkwater, M.J., et al. 2000, PASA, 17, 227

Drinkwater, M.J., et al. 2003, Nature, 423, 519

Driver, S.P., Couch, W.J. & Phillipps, S. 1998, MNRAS, 301, 369

Driver, S. P., Allen, P. D., Liske, J., & Graham, A. W. 2007a, ApJ, 657, L85

Driver, S.P., Popescu, C.C., Tuffs, R.J., Liske, J., Graham, A.W., Allen, P.D., De Propris, R. 2007b, MNRAS, in press (arXiv:0704.2140)

Duc, P.-A., Bournard, F. & Masset, F. 2004, A&A427, 803

Ebisuzaki, T., Makino, J., & Okumura, S.K. 1991, Nature, 354, 212

Edwards, S.A., Colless, M., Bridges, T.J., Carter, D., Mobasher, B. & Poggianti, B.M. 2002, ApJ, 567, 178

Efstathiou, G. 2000, MNRAS, 317, 697

Einasto, J. 1965, Trudy Inst. Astrofiz. Alma-Ata, 5, 87

Einasto, J. 1972, Tartu, Academy of Sciences of the Estonian SSR, Institute of Physics and Astronomy, W. Struve Astrophysical Observatory, 1972., 13

Einasto, J. 1974, Stars and the Milky Way System, 291

Eisenhardt, P.R., De Propris, R., Gonzalez, A.H., Stanford, S.A., Wang, M., & Dickinson, M. 2007, ApJS, 169, 225

Elmegreen, D. M., Elmegreen, B. G., & Bellin, A. D. 1990, ApJ, 364, 415

Elmegreen, B. G., Elmegreen, D. M., & Hirst, A. C. 2004, ApJ, 612, 191

Erwin, P., & Sparke, L. S. 2002, AJ, 124, 65

Erwin, P. 2005, MNRAS, 364, 283

Erwin, P., Vega Beltrán, J. C., Graham, A. W., & Beckman, J. E., & Pohlen, M. 2003, ApJ, 597, 929

Erwin, P., Beckman, J. E., & Pohlen, M. 2005, ApJ, 626, L81

Erwin, P., Pohlen, M., & Beckman, J. E. 2007, AJ, in press

Faber, S.M. & Jackson, R.E. 1976, ApJ, 204, 668

Fellhauer, M. & Kroupa, P. 2002, MNRAS, 330, 642

Fellhauer, M. & Kroupa, P. 2005, MNRAS, 359, 223

Ferguson, H., & Binggeli, B. 1994, ARA&A, 6, 67

Ferguson, H., & Sandage, A. 1989 ApJ, 346, L53

Ferguson, H.C. & Sandage, A.R. 1991, AJ, 101, 765

Ferrarese, L., & Merritt, D. 2000, ApJ, 539, L9

Ferrarese, L., et al. 2006a, ApJS, 164, 334

Ferrarese, L., et al. 2006b, ApJ, 644, L21

Finoguenov, A., Briel, U.G., Henry, J.P., Gavazzi, G., Iglesias-Paramo, J. & Boselli, A. 2004, A&A, 419, 47

Forbes, D., Sánchez-Blázquez, P., & Proctor, R. 2005, MNRAS, 361, 6

Freeman, K. C. 1970, ApJ, 160, 811

Fruchter, A. S., & Hook, R. N. 2002, PASP, 114, 144

Gardner, J.P., Sharples, R.M., Frenk, C.S. & Carrasco, B.E. 1997, ApJ, 480, L99

Gavazzi, G., O'Neil, K., Boselli, A. & van Driel, W. 2006, A&A449, 929

Gebhardt, K., et al. 2000, AJ, 119, 1157

Geller, M.J. & Huchra, J.P. 1989, Science, 246, 897

Godwin, J.G. & Peach, J.V. 1977, MNRAS, 181, 323

Godwin, J.G., Metcalfe, N. & Peach, J.V. 1983, MNRAS, 202, 113

Graham, A.W. 2004, ApJ, 613, L33

Graham, A.W. 2007, MNRAS, in press

Graham, A.W., & Driver, S.P. 2007, ApJ, 655, 77

Graham, A.W., Erwin, P. Caon, N., & Trujillo, I. 2001, ApJ, 563, L11

Graham, A.W., Erwin, P., Trujillo, I., & Asensio-Ramos, A. 2003, AJ, 125, 2951

Graham, A.W., & Guzmán, R. 2003, AJ, 125, 2936

Graham, A.W., Jerjen, H., & Guzmán, R. 2003, AJ, 126, 1787

Gregg, M.D. 1997 New Astronomy, 1, 363

Gualandris, A. & Merritt D. 2007, ApJ, submitted (arXiv:0708.0771)

Gutiérrez, C.M., Trujillo, I., Aguerri, J.A.L., Graham, A.W. & Caon, N. 2004, ApJ, 602, 664

Guzmán. R., Lucey, J.R., Carter, D. & Terlevich, R.J. 1992, MNRAS, 257, 187

Guzmán. R., Lucey, J.R. & Bower, R.G. 1993, MNRAS, 265, 731

Hammer, D. et al. 2008, in preparation.

Harris, W.E., Kavelaars, J.J., Hanes, D.A., Hesser, J.E. & Pritchet, C.J. 2000, ApJ, 533, 137

Häring, N., & Rix, H.-W. 2004, ApJ, 604, L89

Haşegan, M. et al. 2005, ApJ, 627, 203

Hilker, M. 2006, "Globular Clusters - Guides to Galaxies", Concepcion, Chile, eds. T. Richtler & S. Larsen (Springer), see also arXiv:astro-ph/0605447

Hilker, M., Infante, L., Vieira, G., Kissler-Patig, M., & Richtler, T. 1999, A&AS, 134, 75

Hilker, M., Kayser, A., Richtler, T. & Willemsen, P. 2004, A&A, 422, L9

Hjorth, J. & Tanvir, N.R. 1997, ApJ, 482, 68

Hornschemeier, A.E., Mobasher, B., Alexander, D.M., Bauer, F.E., Bautz, M.W., Hammer, D. & Poggianti, B.M. 2006, ApJ, 643, 144

James, P.A., Salaris, M., Davies, J.I., Phillipps, S. & Cassisi, S. 2006, MNRAS, 367, 339

Jenkins, L.P., Hornschemeier, A.E., Mobasher, B., Alexander, D.M. & Bauer, F. E. 2007 ApJ, in press (arXiv:0705.3681v1 [astro-ph])

Jensen, J.B., Tonry, J. & Luppino, G. 1999 ApJ, 510, 71

Jogee, S. 1999, Ph.D. thesis, Yale University

Jogee, S. et. al. 2004, ApJ, 615, L105

Jogee, S., Scoville, N., & Kenney, J. D. P. 2005, ApJ, 630, 837

Jones, J.B. et al. 2006, AJ, 131, 312

Jordán, A. et al. 2005, ApJ, 634, 1002

Jordán, A., et al. 2007, ApJS, 169, 213

Jorgensen, I. 1999, MNRAS, 306, 607

Jorgensen, I., Franx, M. & Kjaergaard, P. 1996, MNRAS, 280, 167

Jorgensen, I., Chiboucas, K., Flint, K., Bergmann, M., Barr, J. & Davies, R.L. 2006, ApJ639, L9

Kaastra, J.S., Lieu, R., Tamura, T., Paerels, F.B.S. & den Herder, J. W. 2003, A&A397, 445

Kavelaars, J.J., Harris, W.E., Hanes, D.A., Hesser, J.E. & Pritchet, C.J. 2000, ApJ, 533, 125

Knapen, J. H. 2005, A&A, 429, 141

Kobayashi, C. 2004, MNRAS, 347, 740

Kochanek, C.S. et al. 2001, ApJ, 560, 566

Koekemoer, A. M., Fruchter, A. S., Hook, R. N., & Hack, W. 2003, in "2002 HST Calibration Workshop", eds. S. Arribas, A. Koekemoer, & B. Whitmore (Baltimore: STScI), 337

Komiyama, Y. et al. 2002, ApJS, 138, 265

Kormendy, J. 1985, ApJ, 295, 73

Kormendy, J. 1988, ApJ, 325, 128

Kormendy, J. & Kennicutt, R.C. 2004, ARA&A, 42, 603

Laine, S., Shlosman, I., Knapen, J. H., & Peletier, R. F. 2002, ApJ, 567, 97

Laurikainen, E., Salo, H., & Buta, R. 2005, MNRAS, 362, 1319

Lieu, R., Mittaz, J.P.D., Bowyer, S., Breen, J.O., Lockman, F.J., Murphy, E.M. & Hwang, C.-Y. 1996, Science, 274, 1335

Lisker, T., Debattista, V. P., Ferreras, I., & Erwin, P. 2006, MNRAS, 370, 477

Lisker, T., Grebel. E.K., Bingelli, B. & Glatt, K. 2007, ApJ, 660, 1186

Lucas, R. A., Swam, M., Mutchler, M., & Sirianni, M. 2006, in "2005 HST Calibration Workshop", eds. A. Koekemoer, P. Goudfrooij, & L. Dressel (Baltimore: STScI), 61

Lucey, J.R., Guzmán, R., Carter, D. & Terlevich, R.J. 1991, MNRAS, 253, 584

Marconi, A., & Hunt, L.K. 2003, ApJ, 589, L21

Marín-Franch, A. & Aparicio, A. 2002, ApJ, 568, 174

Mastropietro, C, Moore, B., Mayer, L., Debattista, V. P., Piffaretti, R. & Stadel, J. 2005, MNRAS, 364, 607

Matković, A. & Guzmán, R. 2005, MNRAS362, 289

Matković, A., Guzmán, R., Sánchez-Blázquez, P., Gorgas, J., Cardiel, N. & Gruel, N. 2007, MNRASsubmitted

Matković, A. & Guzmán, R. 2008, in preparation

McLure, R.J., & Dunlop, J.S. 2002, MNRAS, 331, 795

Mehlert, D., Thomas, D., Saglia, R.P., Bender, R. & Wegner, G. 2003, A&A, 407, 423

Merritt, D. 1984, ApJ, 280, L5

Merritt, D. 2006a, Reports of Progress in Physics, 69, 2513.

Merritt, D. 2006b, ApJ, 648, 976

Merritt, D., Milosavljević, M., Favata, M., Hughes, S. A., & Holz, D. E. 2004, ApJ, 607, L9

Merritt, D., Graham, A.W., Moore, B., Diemand, J., & Terzic, B. 2006, AJ, 132, 2685

Merritt, D., Mikkola, S., & Szell, A. 2007, ArXiv e-prints, 705, arXiv:0705.2745

Mieske, S. et al. 2006, ApJ, 653, 193

Mieske, S., Hilker, M., Infante, L. & Mendes de Oliveira, C. 2007, in "Dark Galaxies and lost Baryons", Proc. I.A.U. symposium 244, eds: J.I. Davies & M.J. Disney, p119, (astro-ph/0707.3869)

Milne, M.L., Pritchet, C.J., Poole, G.B., Gwyn, S.D.J., Kavelaars, J.J., Harris, W.E. & Hanes, D.A. 2007, AJ, 133, 177

Mobasher, B. et al. 2001, ApJS, 137, 279

Mobasher, B. et al. 2003, ApJ, 587, 605

Moore, B., et al. 2006, MNRAS, 368, 563

Moore, B., Katz, N., Lake, G., Dressler, A., & Oemler, A. 1996, Nature, 379, 613

Moore, B., Lake, G. & Katz, N. 1998, ApJ, 495, 139

Moore, S.A.W., Lucey, J.R., Kuntschner, H. & Colless, M. 2002, MNRAS, 336, 382

Navarro, J.F., Frenk, C.S. & White, S.D.M. 1996, ApJ, 462, 563

Nelan, J.E. et al. 2005, ApJ, 632, 137

Neumann, D.M. et al. 2001, A&A, 365, L74

Pavlovsky, C., et al. 2006, "Advanced Camera for Surveys Instrument Handbook for Cycle 16", Version 7.1, (Baltimore: STScI).

Peng, E.W. et al. 2006a, ApJ, 639, 95

Peng, E.W. et al. 2006a, ApJ, 639, 838

Phillipps, S., Driver, S.P., Couch, W.J & Smith, R.M. 1998, ApJ, 498, L119

Phillipps, S., Drinkwater, M.J., Gregg, M. & Jones, J.B. 2001, ApJ, 560, 201

Pipino, A., Puzia, T. H., & Matteucci, F. 2007, ApJ in press, ArXiv e-prints, 704, arXiv:0704.0535

Pohlen, M., & Trujillo, I. 2006, A&A, 454, 759

Poggianti, B.M. et al. 2001, ApJ, 562, 689

Poggianti, B.M. et al. 2004, ApJ, 601, 197

Puzia, T.H., Zepf, S.E., Kissler-Patig, M., Hilker, M., Minniti, D. & Goudfrooij, P. 2002, A&A, 391, 453

Rakos, K. & Schombert, J. 2004, AJ, 127, 1502

Redmount, I. H., & Rees, M. J. 1989, Comments on Astrophysics, 14, 165

Renaud, M., Bélanger, G., Paul, J., Lebrun, F. & Terrier, R. 2006, A&A453, L5

Roberts, S. et al. 2004, MNRAS, 352, 478

Roche, N., Ratnatunga, K., Griffiths, R.E. & Im, M. 1997, MNRAS, 288, 200

Sabatini, S., Davies, J.I., Roberts. S. & Scaramella, R. 2007, in "Dark Galaxies and lost Baryons", Proc. I.A.U. symposium 244, eds: J.I. Davies & M.J. Disney, (astro-ph/0707.4079)

Sánchez-Blázquez, P., Gorgas, J. & Cardiel, N. 2006, A&A, 457, 823

Sembach, K. R., et al. 2006, "HST Two-Gyro Handbook", Version 3.0, (Baltimore: STScI)

Sèrsic, J.L. 1968, Atlas de Galaxias Australes (Córdoba: Obs Astron., Univ. Nac. Córdoba)

Sheth, K., Regan, M. W., Scoville, N. Z., & Strubbe, L. E., 2003, ApJ, 592, L13

Sirianni, M., Martel, A. R., Jee, M. J., Van Orsow, D., & Sparks, W. B. 2003, in "2002 HST Calibration Workshop", eds. S. Arribas, A. Koekemoer, & B. Whitmore (Baltimore: STScI), 82

Sirianni, M., et al. 2005, PASP, 117, 1049.

Smith, R.M., Driver, S.P., & Phillipps, S. 1997, MNRAS, 287, 415

Smith, R.J. et al. 2004, AJ, 128, 1558

Smith, R.J. Hudson, M.J., Lucey, J.R., Nelan J.E. & Wegner, G.A. 2006, MNRAS, 369, 1419

Somerville, R.S. & Primack, J.R. 1999, MNRAS, 310, 1087

Thomsen, B., Baum, W.A., Hammergren, M. & Worthey, G. 1997, ApJ, 483, L37

Tran, K.-V.H., van Dokkum, P., Illingworth, G.D., Kelson, D., Gonzalez, A. & Franx, M. 2005, ApJ, 619, 134

Tremaine, S. 1995, AJ, 110, 628

Trentham, N., Tully, R.B., & Verheijen, M.A.W. 2001, MNRAS, 325, 385.

Trentham, N. & Hodgkin, S. 2002, MNRAS, 333, 423

Trentham, N. & Tully, R.B. 2002, MNRAS, 335, 712

Trujillo, I., Erwin, P., Asensio Ramos, A. & Graham, A.W. 2004, AJ, 127, 1917

Tully, R.B. & Pierce, M.J. 2000, ApJ, 533, 744

Tully, R.B., Somerville, R., Trentham, N. & Verheijen, M.A.W. 2002, ApJ, 569, 573

Valentijn, E.A. et al. 2006, in ADASS XVI ASP Conference Series, 2006, Eds: R. Shaw, F.Hill and D. Bell

Valentijn, E.A. & Verdoes Kleijn, G. 2006, ERCIM News, 65, 20

van den Bergh, S. 2002, AJ, 124, 782

van Dokkum, P. G. 2001, PASP, 113, 1420

van Zee, L., Barton, E. & Skillman, E.D. 2004, AJ, 128, 2797

Varela, J., Moles, M., Márquez, I., Galletta, G., Masegosa, J. & Bettoni, D. 2004, å420, 873

Vogt, N.P., Haynes, M.P., Herter, T., & Giovanelli, R. 2004, AJ, 127, 3273

White, S.D.M., Briel, U.G. & Henry, J.P 1993, MNRAS, 261, L8

Wirth, A. & Gallagher, J.S. 1984, ApJ, 282, 85

Woodworth, S.C. & Harris, W.E. 2000, AJ, 119, 2699

Younger, J. D., Cox, T. J., Seth, A. C., & Hernquist, L. 2007, ApJ, in press

Zheng, X.Z., Hammer, F., Flores, H., Assémat, F. & Rawat, A. 2005, A&A, 435, 507

Zwaan, M.A., Meyer, M.J., Stavely-Smith, L. & Webster, R.L. 2005, MNRAS, 359, 30

Table 6. List of survey fields

Visit	Field	RA (J2000.0)	Dec	Orient	Members	Date of Observation	Dither positions Obtained
1	Coma1_1	13:00:45.90	28:04:54.0	282.0	GMP2440,GMP2449,GMP2489	09/Jan/2007	4
2	Coma1_2	13:00:30.30	28:04:54.0	282.0	GMP2626,GMP2559	09/Jan/2007	4
3	Coma1_3	13:00:14.70	28:04:54.0	282.0	GMP2752,GMP2787,GMP2805,GMP2784,GMP2848,	20/Jan/2007	2
					GMP2861,GMP2879,GMP2922	...	...
4	Coma1_4	12:59:59.10	28:04:54.0	282	GMP3058	...	...
5	Coma1_5	12:59:43.50	28:04:54.0	282	GMP3113,GMP3121,GMP3160	...	...
6	Coma7_6	12:59:06.30	27:45:48.0	282	GMP3660,GMP3730,GMP3739,GMP3750	...	...
7	Coma1_7	12:59:12.30	28:04:54.0	282	GMP3561,GMP3554,GMP3656	...	...
8	Coma2_1	13:00:42.30	28:01:43.0	282.0	GMP2417,GMP2423,GMP2511,GMP2529,GMP2551,	12/Jan/2007	4
					GMP2550,GMP2559	...	...
9	Coma2_2	13:00:26.70	28:01:43.0	282.0	GMP2676,GMP2727,GMP2777	13/Jan/2007	4
10	Coma2_3	13:00:11.10	28:01:43.0	282.0	GMP2839,GMP2856,GMP2940,GMP2960	13/Jan/2007	4
11	Coma2_4	12:59:55.50	28:01:43.0	282	GMP3073	...	...
12	Coma2_5	12:59:39.90	28:01:43.0	282.0	GMP3312	12/Jan/2007	3
13	Coma2_6	12:59:24.30	28:01:43.0	282.0	GMP3390,GMP3406,GMP3433,GMP3438,GMP3471	13/Jan/2007	2
14	Coma2_7	12:59:08.70	28:01:43.0	282.0	GMP3681,GMP3707,GMP3762,GMP3780,GMP3811	08/Jan/2007	3
15	Coma3_1	13:00:38.70	27:58:32.0	282.0	GMP2510,GMP2516,GMP2535	26/Jan/2007	4
16	Coma3_2	13:00:23.10	27:58:32.0	282.0	GMP2651,GMP2654,GMP2718,GMP2799,GMP2815,	25/Jan/2007	4
					GMP2794,GMP2798	...	...
17	Coma3_3	13:00:07.50	27:58:32.0	282	GMP2929,GMP2921,GMP2946,GMP2964,GMP2965,	...	...
					GMP2985,GMP2940	...	...
18	Coma3_4	12:59:51.90	27:58:32.0	282.0	GMP3018,GMP3098,GMP3146,GMP3166,GMP3170,	25/Jan/2007	4
					GMP3206	...	...
19	Coma3_5	12:59:36.30	27:58:32.0	282.0	GMP3206,GMP3213,GMP3254,GMP3269,GMP3291,	25/Jan/2007	4
					GMP3292,GMP3308,GMP3329,GMP3367,GMP3414	...	...
20	Coma3_6	12:59:20.70	27:58:32.0	282	GMP3471,GMP3484,GMP3487,GMP3489,GMP3515,	...	...
					GMP3534,GMP3565,GMP3602,GMP3615,GMP3639	...	...
21	Coma3_7	12:59:05.10	27:58:32.0	282	GMP3664,GMP3761,GMP3851,GMP3877,GMP3794	...	...
22	Coma4_1	13:00:35.10	27:55:21.0	282.0	GMP2541,GMP2563,GMP2571,GMP2585,GMP2591	22/Jan/2007	4
23	Coma4_2	13:00:19.50	27:55:21.0	282.0	GMP2692,GMP2736,GMP2780,GMP2778	27/Jan/2007	4
24	Coma4_3	13:00:03.90	27:55:21.0	282.0	GMP2931,GMP3017,GMP3034	24/Jan/2007	4
25	Coma4_4	12:59:48.30	27:55:21.0	282.0	GMP3068,GMP3080,GMP3133,GMP3131,GMP3201,	24/Jan/2007	4
					GMP3215,GMP3222	...	...
26	Coma4_5	12:59:32.70	27:55:21.0	282	GMP3296,K9992,GMP3325,GMP3340,GMP3352,	...	...

Table 6—Continued

Visit	Field	RA (J2000.0)	Dec (J2000.0)	Orient	Members	Date of Observation	Dither positions Obtained
					GMP3376,GMP3424	...	...
27	Coma4_6	12:59:17.10	27:55:21.0	282	GMP3486,GMP3510,GMP3511,GMP3522,GMP3645	...	...
28	Coma4_7	12:59:01.50	27:55:21.0	282	GMP3719,GMP3782,GMP3855	...	...
29	Coma5_1	13:00:31.50	27:52:10.0	282	GMP2716	...	...
30	Coma5_2	13:00:15.90	27:52:10.0	282	GMP2716,GMP2753,GMP2852,GMP2897,GMP2910,	...	...
					GMP2913	...	...
31	Coma5_3	13:00:00.30	27:52:10.0	282	GMP2910,GMP3052	...	...
32	Coma5_4	12:59:44.70	27:52:10.0	282	GMP3178,GMP3196,GMP3205	...	...
33	Coma5_5	12:59:29.10	27:52:10.0	282.0	GMP3311,GMP3339,GMP3383,GMP3400,GMP3423,	15/Jan/2007	4
					GMP3473	...	...
34	Coma5_6	12:59:13.50	27:52:10.0	282	GMP3557,GMP3645,GMP3706,GMP3719,GMP3733	...	...
35	Coma5_7	12:58:57.90	27:52:10.0	282	GMP3821,GMP3911,GMP3946	...	...
36	Coma6_1	13:00:27.90	27:48:59.0	282	GMP2603	...	...
37	Coma6_2	13:00:12.30	27:48:59.0	282	GMP2783,GMP2800,GMP2956	...	...
38	Coma6_3	12:59:56.70	27:48:59.0	282	GMP3092,GMP3122,GMP3126	...	...
39	Coma6_4	12:59:41.10	27:48:59.0	282	GMP3126,GMP3313,GMP3324	...	...
40	Coma6_5	12:59:25.50	27:48:59.0	282	GMP3403,GMP3411,GMP3425	...	...
41	Coma6_6	12:59:09.90	27:48:59.0	282	...	...	...
42	Coma6_7	12:58:54.30	27:48:59.0	282	GMP3895,GMP3896,GMP3898,GMP3925,GMP3943,	...	...
					GMP3949,GMP3997	...	...
43	Outskirts_1	12:57:56.90	27:28:55.0	239-241	GMP4522,GMP4597,GMP4630	...	...
44	Outskirts_2	12:58:01.70	27:25:48.0	265-270	GMP4479,GMP4535,GMP4577,GMP4568	...	...
45	Outskirts_3	12:58:21.58	27:27:40.7	318.0	GMP4206,GMP4330,GMP4381	21/Nov/2006	4
46	Outskirts_4	12:58:34.00	27:22:58.8	280.0	GMP4192,GMP4215	17/Jan/2007	4
47	Outskirts_5	12:57:27.38	27:28:59.1	219-221	GMP4792,GMP4794,GMP4928,GMP4943,GMP4956	...	...
48	Outskirts_6	12:58:00.50	27:22:23.7	238-290	GMP4484,GMP4545,GMP4565,GMP4578	...	...
49	Outskirts_7	12:57:42.52	27:26:37.6	280-323	GMP4692,GMP4712,GMP4768	...	...
50	Outskirts_8	12:57:27.40	27:23:37.0	230-323	GMP4910,GMP4918	...	...
51	Outskirts_9	12:57:04.70	27:21:25.1	260-323	GMP5076,GMP5136	...	...
52	Outskirts_10	12:56:44.30	27:26:12.0	250-323	GMP5250,GMP5255,GMP5296	...	...
53	Outskirts_11	12:57:55.25	27:13:55.7	any	GMP4591	...	...
54	Outskirts_12	12:56:37.81	27:33:08.4	215-255	GMP5284,GMP5320,GMP5364	...	...
55	Outskirts_13	12:57:04.22	27:31:34.5	299.1	GMP5102	19/Jan/2007	4
56	Outskirts_14	12:57:26.40	27:32:54.4	220-323	GMP4852,GMP4907,GMP4937	...	...

Table 6—Continued

Visit	Field	RA (J2000.0)	Dec (J2000.0)	Orient	Members	Date of Observation	Dither positions Obtained
57	Outskirts_15	12:58:02.08	27:33:54.0	250-260	GMP4447,GMP4469,GMP4579	···	···
58	Outskirts_16	12:58:34.59	27:33:43.3	220-225	GMP4117,GMP4156,GMP4255	···	···
59	Outskirts_17	12:58:31.15	27:11:58.5	270.05	GMP4135,GMP4259,GMP4294	16/Jan/2007	4
60	Outskirts_18	12:58:15.55	27:05:15.1	any	GMP4383	···	···
61	Outskirts_19	12:58:48.72	28:00:52.8	265-323	GMP3969,GMP3973,GMP4003	···	···
62	Outskirts_20	12:56:36.03	26:54:17.8	any	GMP5361	···	···
63	Outskirts_21	12:56:29.80	27:13:32.8	265.0	GMP5335,GMP5359,GMP5365,GMP5472	21/Jan/2007	4
64	Outskirts_22	12:57:56.51	27:02:16.4	any	GMP4582,GMP4596	···	···
65	Outskirts_23	12:57:21.08	27:00:04.2	220-260	GMP4961,GMP4980,GMP4947	···	···
66	Outskirts_24	12:57:08.88	27:05:47.8	200-290	GMP5032,GMP5097	···	···
67	Outskirts_25	12:56:37.84	27:02:49.3	230-250	GMP5283,GMP5293,GMP5294,GMP5395	···	···
68	Outskirts_26	12:57:14.03	27:15:14.7	any	GMP5012,GMP5019	···	···
69	Outskirts_27	12:59:12.21	27:36:56.9	265	GMP3585,GMP3598,GMP3696	···	···
70	Outskirts_28	12:57:21.38	27:37:42.1	240-250	GMP4888,GMP4905,GMP4967,GMP4987	···	···
71	Outskirts_29	12:56:29.63	27:42:27.2	250-295	GMP5345,GMP5362,GMP5434	···	···
72	Outskirts_30	12:55:38.57	27:44:39.9	284-286	GMP5850,GMP5912	···	···
73	Outskirts_31	12:57:03.95	27:45:06.4	225-235	GMP5096,GMP5100	···	···
74	Outskirts_32	12:58:25.87	26:54:23.2	245-255	GMP4183,GMP4340	···	···
75	Coma7_7	12:58:47.75	27:46:12.7	280.0	GMP3949,GMP3958,GMP4035,GMP4060	17/Jan/2007	4
76	Outskirts_34	12:58:19.13	27:45:44.6	any	GMP4341,GMP4364	···	···
77	Outskirts_35	12:58:03.52	27:40:57.8	any	GMP4502,GMP4557	···	···
78	Outskirts_36	12:57:10.80	27:24:18.0	314.52	GMP5038	27/Nov/2006	4
79	Outskirts_37	12:57:50.52	27:38:38.8	any	GMP4632	···	···
80	Outskirts_38	12:56:04.00	27:09:03.0	any	GMP5676	···	···
81	Outskirts_39	12:59:50.50	27:44:48.9	230	GMP3071,GMP3132,GMP3176,GMP3192,GMP3195,	···	···
					GMP3211	···	···
82	Outskirts_40	12:56:14.60	27:30:23.2	any	GMP5546	···	···